OPEN ACCESS Freely available online

PLOS ONE

α-Mangostin Disrupts the Development of *Streptococcus mutans* Biofilms and Facilitates Its Mechanical Removal

Phuong Thi Mai Nguyen[1]*, Megan L. Falsetta[2], Geelsu Hwang[3], Mireya Gonzalez-Begne[2], Hyun Koo[2,3]*

1 Institute of Biotechnology, Vietnam Academy of Science and Technology, Hanoi, Vietnam, **2** Center for Oral Biology, University of Rochester Medical Center, Rochester, New York, United States of America, **3** Biofilm Research Labs, Levy Center for Oral Health, Department of Orthodontics, School of Dental Medicine, University of Pennsylvania, Philadelphia, Pennsylvania, United States of America

Abstract

α-Mangostin (αMG) has been reported to be an effective antimicrobial agent against planktonic cells of *Streptococcus mutans*, a biofilm-forming and acid-producing cariogenic organism. However, its anti-biofilm activity remains to be determined. We examined whether αMG, a xanthone purified from *Garcinia mangostana* L grown in Vietnam, disrupts the development, acidogenicity, and/or the mechanical stability of *S. mutans* biofilms. Treatment regimens simulating those experienced clinically (twice-daily, 60 s exposure each) were used to assess the bioactivity of αMG using a saliva-coated hydroxyapatite (sHA) biofilm model. Topical applications of early-formed biofilms with αMG (150 μM) effectively reduced further biomass accumulation and disrupted the 3D architecture of *S. mutans* biofilms. Biofilms treated with αMG had lower amounts of extracellular insoluble and intracellular iodophilic polysaccharides (30–45%) than those treated with vehicle control ($P<0.05$), while the number of viable bacterial counts was unaffected. Furthermore, αMG treatments significantly compromised the mechanical stability of the biofilm, facilitating its removal from the sHA surface when subjected to a constant shear stress of 0.809 N/m^2 (>3-fold biofilm detachment from sHA vs. vehicle-treated biofilms; $P<0.05$). Moreover, acid production by *S. mutans* biofilms was disrupted following αMG treatments (vs. vehicle-control, $P<0.05$). The activity of enzymes associated with glucan synthesis, acid production, and acid tolerance (glucosyltransferases B and C, phosphotransferase-PTS system, and F_1F_0-ATPase) were significantly inhibited by αMG. The expression of *manL*, encoding a key component of the mannose PTS, and *gtfB* were slightly repressed by αMG treatment ($P<0.05$), while the expression of *atpD* (encoding F-ATPase) and *gtfC* genes was unaffected. Hence, this study reveals that brief exposures to αMG can disrupt the development and structural integrity of *S. mutans* biofilms, at least in part via inhibition of key enzymatic systems associated with exopolysaccharide synthesis and acidogenicity. αMG could be an effective anti-virulence additive for the control and/or removal of cariogenic biofilms.

Citation: Nguyen PTM, Falsetta ML, Hwang G, Gonzalez-Begne M, Koo H (2014) α-Mangostin Disrupts the Development of *Streptococcus mutans* Biofilms and Facilitates Its Mechanical Removal. PLoS ONE 9(10): e111312. doi:10.1371/journal.pone.0111312

Editor: Jens Kreth, University of Oklahoma Health Sciences Center, United States of America

Received July 7, 2014; **Accepted** September 19, 2014; **Published** October 28, 2014

Data Availability: The authors confirm that all data underlying the findings are fully available without restriction. All relevant data are within the paper and its Supporting Information files.

Funding: This work was supported by National Foundation for Science and Technology Development (Nafosted) grant (106.05-2011.44) to PTMN (http://www.nafosted.gov.vn); Vietnam Education Foundation (VEF) research scholar grant (VEF 2012) to PTMN (https://home.vef.gov); and National Institutes of Health (NIH) grant (DE018023) to HK. The funders had no role in study design, data collection and analysis, decision to publish, or preparation of the manuscript.

Competing Interests: The authors have declared that no competing interests exist.

* Email: koohy@dental.upenn.edu (HK); phuong_nguyen_99@yahoo.com (PTMN)

Introduction

Many infectious diseases in human are caused by virulent biofilms, including oral diseases [1]. Among them, dental caries continues to be one of the most ubiquitous and costly biofilm-dependent diseases throughout the world [2,3]. For organisms associated with caries development, the production of an extracellular polysaccharide (EPS)-rich biofilm matrix, acidification of the milieu, and the maintenance of acidic pH microenvironment in close proximity to the tooth enamel are major controlling virulence factors linked with the pathogenesis of the disease. Current therapeutic approaches to control pathogenic oral biofilms fall short; the search for new/improved agents may lead to more efficacious anti-caries therapies [4–6]. Natural products are currently regarded as potentially promising sources for new bioactive agents that may function to suppress these key virulence attributes that are associated with the establishment and maintenance of cariogenic biofilms [5].

The assembly of cariogenic biofilms results from complex interactions that occur between specific oral bacteria, the products they produce, host saliva and dietary carbohydrates, all of which occurs on pellicle-coated tooth surfaces [7,8]. *Streptococcus mutans* has been recognized as one of the key etiologic agents associated with the initiation of dental caries, although additional organisms may contribute to its pathogenesis [9]. Sucrose is considered the primary catalyst for caries development, as it serves as a substrate for the production of both EPS and acids. *S. mutans* can effectively form cariogenic biofilms when sucrose is available, because this bacterium rapidly synthesizes EPS (from sucrose) through the activity of exoenzymes (e.g. glucosyltransferases; Gtfs) [8]. At the same time, *S. mutans* produces acid and is highly aciduric, allowing it to tolerate and continue to produce acids in low pH

microenvironments, while readily adapting to acidic and other environmental stresses [10–14].

EPS synthesis via *S. mutans*-derived Gtfs is critical for cariogenic biofilm formation, since the glucans produced by the secreted exoenzymes (present in the pellicle-coated tooth and on bacterial surfaces) promote local bacterial accumulation, while embedding bacteria in a diffusion-limiting matrix. These processes create highly cohesive and adhesive biofilms that are firmly attached to surfaces and are difficult to remove [15–18]. At the same time, the EPS-rich matrix shelters resident organisms from antimicrobial and other inimical influences [18–20]. In parallel, sugars (in addition to sucrose) are fermented by *S. mutans* and other acidogenic bacteria ensnared within the biofilm matrix, creating acidic microenvironments across the three-dimensional (3D) architecture and at the surface of attachment [18,21,22]. Acidification of the milieu favors growth of aciduric organisms, further enhancing EPS production and ensuring biofilm accrual and localized acid-dissolution of the enamel in areas where biofilm is present and pH is low [18,23]. Therefore, using bioactive agents that target EPS-mediated biofilm assembly and acidogenicity could disrupt the pathogenesis of dental caries in a highly effective and precise manner.

Plants are valuable sources of new bioactive compounds to combat dental caries, because they produce a wide variety of secondary metabolites, many of which have been found to have biological properties against oral pathogens *in vitro* (as reviewed in Jeon et al. [5]). *Garcinia mangostana* L. (Guttiferae) is a widely cultivated fruit tree in Southeast Asian nations, including Thailand, Sri Lanka, The Philippines, and Vietnam [24]. The pericarp of *G. mangostana* has been used in traditional medicine to treat a variety of infections. Experimental studies have demonstrated that xanthone derivatives are the major bioactive substances, exhibiting antioxidant, antitumor, anti-inflammatory, and antimicrobial activities [24–26].

Our previous work showed that αMG exhibits antimicrobial activity against planktonic *S. mutans* cells via multiple actions, particularly reducing acid production by disrupting the membrane of this organism [27]. However, the question as to whether this agent is capable of compromising the ability of *S. mutans* to develop biofilms using a clinically relevant treatment regiment (brief topical exposures) remains to be elucidated. Therefore, the aim of the present study was to investigate the potential effectiveness of topical applications of αMG and its biological actions against *S. mutans* biofilm formation on saliva-coated apatitic surfaces.

Materials and Methods

Extraction and isolation of α-mangostin

Garcinia mangostana L is a fruit plant widely available in the south of Vietnam. The dried powder of samples of *Garcinia mangostana* peels collected from Binhduong province (south of Vietnam) was used in this study. No specific permission for collection of *G. mangostana* is required for this location because it is not an endangered or protected species. Ethanolic extracts of *G. mangostana* were prepared for the initial step of αMG isolation. The dried powder of *G. mangostana* peels collected from the South of Vietnam were extracted with ethanol at room temperature, followed by an evaporation of solvent to give a dark brown gummy residue. This residue was taken up in water followed by extraction with *n*-hexane to produce the most bioactive fractions. The *n*-hexane fraction was then evaporated and dried under reduced pressure. Further separation was performed using silica gel column chromatography (Merck Kieselgel 60, 70–230 mesh) by eluting with *n*-hexane – ethyl acetate – methanol (6:3:0.1, by volume) and 10 mL volumes of eluant were collected in test tubes. The aliquots of each fraction were subjected to thin-layer chromatography (60 F254, 1 mm plate, Merck) in a solvent system containing toluene – ethyl acetate – acetone – formic acid (5:3:1:1, by volume). Partially purified αMG was recovered from the active fractions and then further separated by silica gel column chromatography (Merck Kieselgel 60, 70–230 mesh) and eluting with *n*-hexane – chloroform – ethyl acetate – methanol (4:1:0.5:0.3, by volume), yielding a single compound, αMG, as yellow crystals. The purity of αMG was examined by high-pressure liquid chromatography connected with mass spectrometry (LCMSD- Trap-SL Mass spectra, Agilent 1100, Palo Alto, California). The chemical structure (Fig. 1) of αMG was determined using nuclear magnetic resonance (Bruker Avance 500 spectrometer, Germany).

The compound at concentration of 100, 150 and 200 μM was dissolved in 25% ethanol, which was also used as a vehicle control; treatments with 25% ethanol did not affect the viability of cells of *S. mutans* in a biofilm when compared to untreated controls. The pH of the treatment solution was maintained at 5.8±0.2, based on the observation that αMG activity is best at acidic pH [27].

Preparation and treatment of the biofilm

S. mutans UA159 (ATCC 700610), a proven virulent-cariogenic strain selected for genomic sequencing, was used in this study. Biofilms of *S. mutans* were formed on saliva coated hydroxyapatite (sHA) surfaces (12.7 mm in diameter, 1 mm in thickness, Clarkson Chromatography Products Inc., South Williamsport, PA), as previously described [28]. The biofilms were grown in ultra-filtered (10 kDa MW cut-off membrane; Prep/Scale, Millipore, MA) buffered tryptone-yeast extract broth (UFTYE; 2.5% tryptone and 1.5% yeast extract with the addition of 4.35 g/L of potassium phosphate and 1 g/L of $MgSO_4 \cdot 7H_2O$, pH 7.0) with 1% sucrose at 37°C and 5% CO_2. Briefly, *S. mutans* cells in exponential growth phase were inoculated into UFTYE and applied to wells containing sHA discs placed vertically in a custom-made holder. Biofilms were allowed to form on sHA discs and were treated for the first time with the test agents or vehicle control after 6 h of development. Subsequently, the biofilms were treated at 8 am (20 h-old) and 6 pm (30 h-old), with two more additional treatments the following day (8 am; 44 h-old and 6 pm; 54 h-old). The biofilms were exposed to the treatments for 60 s, dip-washed in sterile saline solution (0.89% w/v NaCl) to remove excess agents, and then transferred to fresh culture medium [29,30]. The biofilm was analyzed after 44 h and 68 h using confocal microscopy to examine the effects on the overall 3D architecture after receiving the initial topical treatments (Figure 2). At 68 h, the biofilms were removed, homogenized and subjected to biochemical analysis as detailed previously [28]. Briefly, biomass was assessed with an aliquot of the homogenized suspension centrifuged at 10,000 *g* for 10 min at 4°C, and the cell pellet was washed twice with water, then dried in the dry oven at 105°C for 24 h and weighed [28]. The water soluble and insoluble exopolysaccharides (EPS), and intracellular iodophilic polysaccharides (IPS) were extracted and quantified via colorimetric assays [28]. The total number of viable cells in each of the biofilms was determined by counting colony forming units (CFU), while total protein was quantified via ninhydrin assays as descrbed in Koo et al. [28]. Furthermore, the pH of the culture media of treated and untreated biofilms was monitored every 2 hours with an Orion pH electrode attached to an Orion 290 A+ pH meter (Thermo Fisher Scientific).

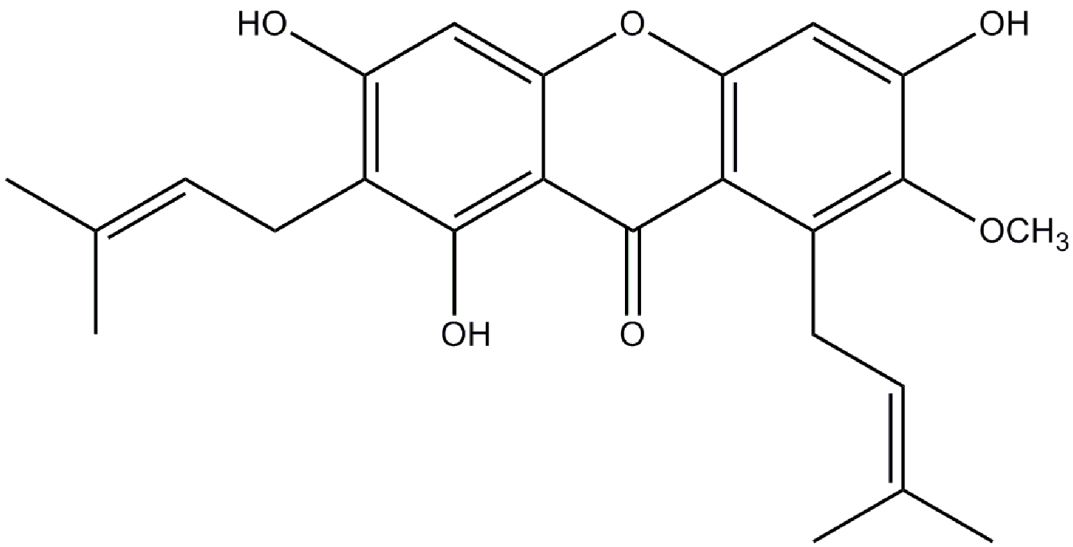

Figure 1. Chemical structure for αMG. Molecular formula: $C_{24}H_{26}O_6$. Molecular weight: 410.466.
doi:10.1371/journal.pone.0111312.g001

Confocal microscopy of biofilms

The overall effect of topical applications of αMG on the 3D architecture and the spatial distribution of EPS and bacterial biomass within intact biofilms was assessed using confocal fluorescence imaging [18]. Briefly, 2.5 μM Alexa Fluor 647-labeled dextran conjugate (10,000 MW; absorbance/fluorescence emission maxima 647/668 nm; Molecular Probes Inc., Eugene, OR) was added to the culture medium during the formation and development of *S. mutans* biofilms. The fluorescently-labeled dextran serves as a primer for Gtf-mediated glucan synthesis and can be simultaneously incorporated during EPS matrix synthesis over the course of biofilm development, but does not stain the bacterial cells at the concentrations used in the study. The bacterial cells in the biofilms were labeled with 2.5 μM SYTO 9 green-fluorescent nucleic acid stain (480/500 nm; Molecular Probes Inc., Eugene, OR) using standard procedures [18]. Laser scanning confocal fluorescence imaging of the biofilms was performed using an Olympus FV 1000 two-photon laser scanning microscope (Olympus, Tokyo, Japan) equipped with a 10 X (0.45 numerical aperture) water immersion objective lens. Each biofilm was scanned at 5 randomly selected positions on the microscope stage and the confocal image series were generated by optical sectioning at each of these positions. Three independent experiments were conducted. The step size of z-series scanning was 2 μm. The confocal images were analyzed using software for simultaneous visualization of EPS and bacterial cells within intact biofilms [18,31,32]. Amira 5.4.1 software (Visage Imaging, San Diego, CA) was used to create 3D renderings of each structural component (EPS and bacteria) to examine the architecture of the biofilm.

Determination of mechanical stability of biofilms

The mechanical stability of the biofilms treated with or without αMG was compared using a custom built device (detailed information is in Figure S1). Biofilms were exposed to constant shear stress of 0.809 N/m^2 for 10 min, which is capable of removing *S. mutans* biofilm from sHA surface; such shear stress was determined as a threshold for >50% removal of untreated *S. mutans* biofilms from saliva-coated HA surfaces using our model. Shear stress at the biofilm surface was produced by shear flow generated via rotating paddle, and estimated based on Reynolds number of the flow (turbulent flow) and the surface friction using Blasius formula (Supplemental information). The amount of biofilm dry-weight (biomass) before and after application of shear

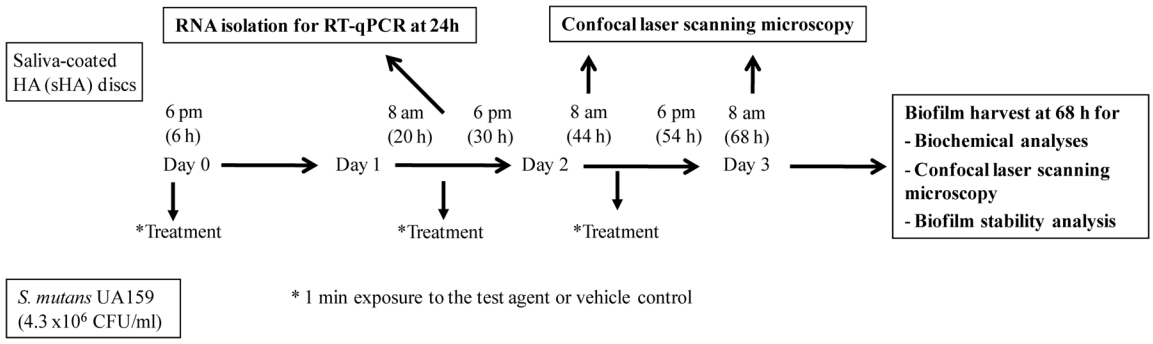

Figure 2. The experimental design for the treatment and analysis of biofilms of *S. mutans*. The clinical conditions of typical exposure of exogenously introduced therapeutic agents in the mouth were simulated by applying the test agent twice daily for brief exposures (60 s) at early/initial formation of the biofilm (6 h). Subsequently, the biofilms were treated twice at 8 am (20 h-old) and 6 pm (30 h-old) with two more additional treatments the following day (8 am; 44 h-old and 6 pm; 54 h-old).
doi:10.1371/journal.pone.0111312.g002

Table 1. *Streptococcus mutans* UA159 biofilm composition after treatments with 150 μM αMG.

Biofilm composition	Vehicle	150 μM αMG
Dry weight (mg/biofilm)	4.73±0.41	3.00±0.45*
Protein (mg/biofilm)	2.85±0.38	1.67±0.19*
Soluble EPS (μg/biofilm)	326.6±37.2	229.7±91.0
Insoluble EPS (μg/biofilm)	1112.1±151.7	356.9±49.0*
IPS (μg/biofilm)	188.3±17.8	79.9±22.6*
CFU/biofilm	2.77E+08±5.98E+07	2.25E+08±5.50E+07

Data are expressed as the mean ± one standard deviation. For each parameter, values marked with an asterisk are significantly different from that for the vehicle control (n = 8; $P<0.05$, pair-wise comparison using Student's t test).

doi:10.1371/journal.pone.0111312.t001

stress for each condition (vehicle- and αMG-treated) was determined. Then, the percentage of biofilm that remained on sHA disc surface was calculated. All experiments were performed in quadruplicates in three distinct experiments.

Gtf Docking Analyses

In the present study, different bioinformatics tools and databases were used. The crystal structure of glucosyltransferases C (GtfC) from the dental caries pathogen *Streptococcus mutans* is available in the Protein Data Bank (PDB) and was used as a receptor for docking of the αMG compound (ligand) using HEX software. Since the crystal structure of GtfB is not yet available, Phyre server [33] was used to predict ligand sites. HEX has been reported as an interactive molecular graphic program. It calculates protein-ligand docking, assuming that the ligand is rigid and then superimposes pairs of molecules using only their 3D shapes [34,35]. In addition, it uses Spherical Polar Fourier (SPF) correlations, increasing the speed of the calculations, and it also has integrated graphics software to view the final result [35–38]. PDB was used to download the crystal structure of glucansucrase from the dental caries pathogen *Streptococcus mutans* (http://www.rcsb.org/pdb/home/home.do). PubChem Compound was used for retrieving the 3D-structure of α-mangostin (http://www.ncbi.nlm.nih.gov/pccompound). MarvinSketch software was utilized for obtaining the α-mangostin structure in a PDB format (http://www.chemaxon.com/products/marvin/marvinsketch/), and the Hex-Server (HEX 6.9 software) was accessed for calculating and displaying protein-ligand docking (http://hexserver.loria.fr/). The parameters used for docking included: Correlation type (Shape only), FFT mode (3D fast life), Grid dimension (0.6), Receptor range (180), Ligand range (180), Twist range (360), and Distance range (40) were used.

Determination of Gtf activity

GtfB and GtfC were obtained from recombinant strains carrying the appropriate genes as detailed elsewhere [34]. Strain *S. milleri* KSB8 harboring the *gtf*B gene transformed from *S. mutans* GS-5 and *S. mutans* WHB 410 construct expressing *gtf*C gene only were used. The GtfB and GtfC enzymes (E.C. 2.4.1.5) were prepared from culture supernatants and purified to near homogeneity by hydroxyapatite column chromatography. The purified Gtfs (1–1.5 U) were mixed with the test compound and incubated with a [U-^{14}C-glucose]-sucrose substrate (0.2 μCi/ml; 200.0 mmol of sucrose per liter, 40 μmol of dextran 9000 per liter, and 0.02% sodium azide in adsorption buffer consisting of 50 mM KCl, 1.0 mM KPO_4, 1.0 mM $CaCl_2$, and 0.1 mM $MgCl_2$, pH 6.5) to a final concentration of 100 mmol of sucrose per liter (200 μl final volume) at 37°C with rocking for 4 h. For the vehicle-control, the same reaction was carried out with 25% ethanol (v/v) replacing the test agent solutions. Glucosyltransferase activity was measured by incorporation of [U-^{14}C-glucose] from labeled sucrose into glucans [34]. The radiolabelled glucans were quantified by scintillation counting.

F-ATPase and phosphotransferase system (PTS) assays

F-ATPase and PTS activity of treated biofilm cells were determined as described by Belli and Marquis [39] and Phan et al. [40]. Biofilms were homogenized and centrifuged at 4°C, and then biofilm pellets from each sample were resuspended in 2.5 ml of 75 mM Tris-HCl buffer (pH 7.0) with 10 mM $MgSO_4$. Toluene (250 ul) was added to each biofilm cell suspension prior to vigorous vortex mixing and incubation for 5 min at 37°C. Each suspension was then subjected to two cycles of freezing in a dry ice-ethanol bath and thawing at 37°C. Permeabilized biofilm cells were harvested by centrifugation. They were then resuspended in 1.0 ml of 75 mM Tris-HCl buffer (pH 7.0) with 10 mM $MgSO_4$. The suspension was quickly frozen in a dry ice-ethanol bath and stored at −70°C for F-ATPase and PTS assays. F-ATPase activity was determined as described by Belli and Marquis [39]. The F-ATPase reaction is initiated by the addition of 30 μl of 0.5 M ATP (pH 6.0). Samples of 50 μl were removed and assayed for inorganic phosphate liberated from cleavage of ATP with reagents from American Monitor Co. (Indianapolis, IN) [39]. Phosphotransferase system (PTS) activity was assessed in terms of pyruvate production from phosphoenolpyruvate in response to glucose addition. Pyruvate was assayed by use of lactic dehydrogenase and measurements of the change in absorbance of 340 nm light associated with oxidation of NADH [39].

Reverse transcription quantitative PCR (RT-qPCR)

RT-qPCR was performed to evaluate the expression of the *gtfB, gtfC, atpD*, and *manL* genes. Biofilms were treated as described in the Figure 2. RNA was extracted and purified using standard protocols optimized for biofilms [41]. The RNA integrity numbers (RIN) of purified samples used for RT-qPCR were determined by microcapillary electrophoresis on an Agilent 2100 Bioanalyzer (Agilent Technologies, Santa Clara, CA). Purified RNA samples (RIN≥9) were stored in RNase-free water at −80°C. cDNAs were synthesized from 1 μg of purified RNA using a BioRad iScript cDNA synthesis kit (Bio-Rad Laboratories, Inc., Hercules, CA). RNA samples without reverse transcriptase were included as a negative control. The resulting cDNAs and negative controls were amplified by a MyiQ qPCR detection system with iQ SYBR Green supermix (Bio-Rad Laboratories, Inc., CA, USA) and specific primers. When Taqman probes were available, cDNAs and controls were amplified using a Bio-Rad CFX96

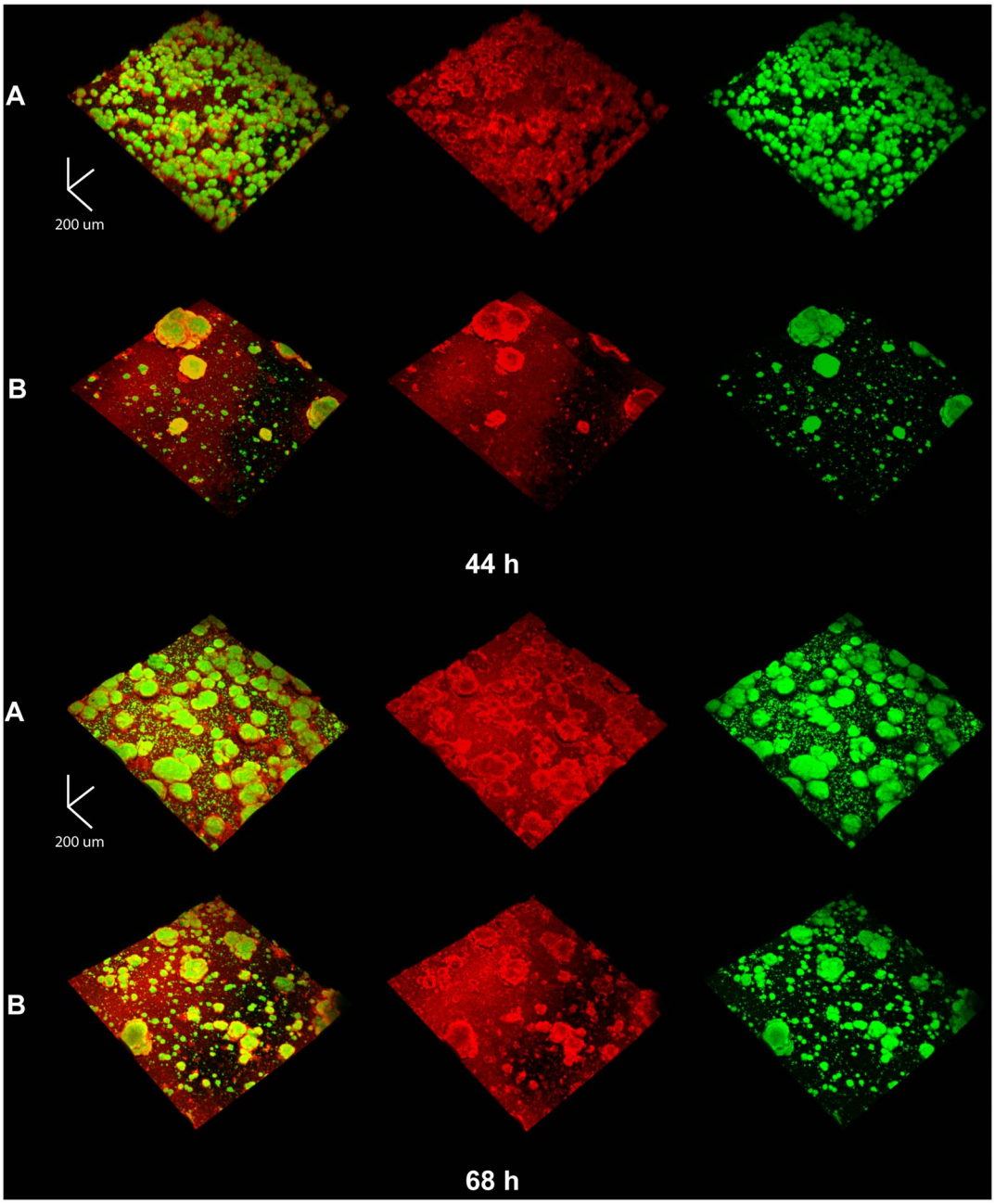

Figure 3. Representative 3D rendered images of 44 h and 68 h-old *S. mutans* biofilms following topical treatments. Biofilms were treated with the vehicle control in panel A and with 150 μM αMG in panel B. The EPS channel is in red, while bacterial cells are in green. Scale bars = 100 μm. Biofilms were formed on hydroxyapatite discs (sHA) in the presence of 1% (wt/vol) sucrose, and treated with test agents twice daily. doi:10.1371/journal.pone.0111312.g003

system (Bio-Rad Laboratories). The 16S rRNA primers/TaqMan probes were run separately, and primers/TaqMan probes for other specific targets were combined and used in a multiplex setting. For reactions with only one TaqMan probe (used for target 16S rRNA), the iQ Supermix (BioRad) was used. For multiplex reactions (*gtfB*, *gtfC*) and (*atpD*, *manL*) the iQ Multiplex Powermix (BioRad) were employed. Standard curves were used to determine the relative number of cDNA molecules, which were normalized to the relative number of 16S rRNA cDNA in each sample, as described previously [42]. 16S rRNA served as a reference gene [43]. These values were used to determine the fold-change between each treated sample and the vehicle control. The MIQE guidelines [44] were followed for quality control of the data generated and for data analysis. The gene expression profile was determined 4 h after the topical treatment at 20 h (Figure 2), to evaluate the impact of αMG on *S. mutans* within the accumulated biofilms post-treatment. This time point represents the most active period of the biofilm development using our model, and was selected based on our biochemical data and previous studies on the dynamics of the *S. mutans* transcriptome during biofilm formation on sHA and in response to topically applied agents [43,45].

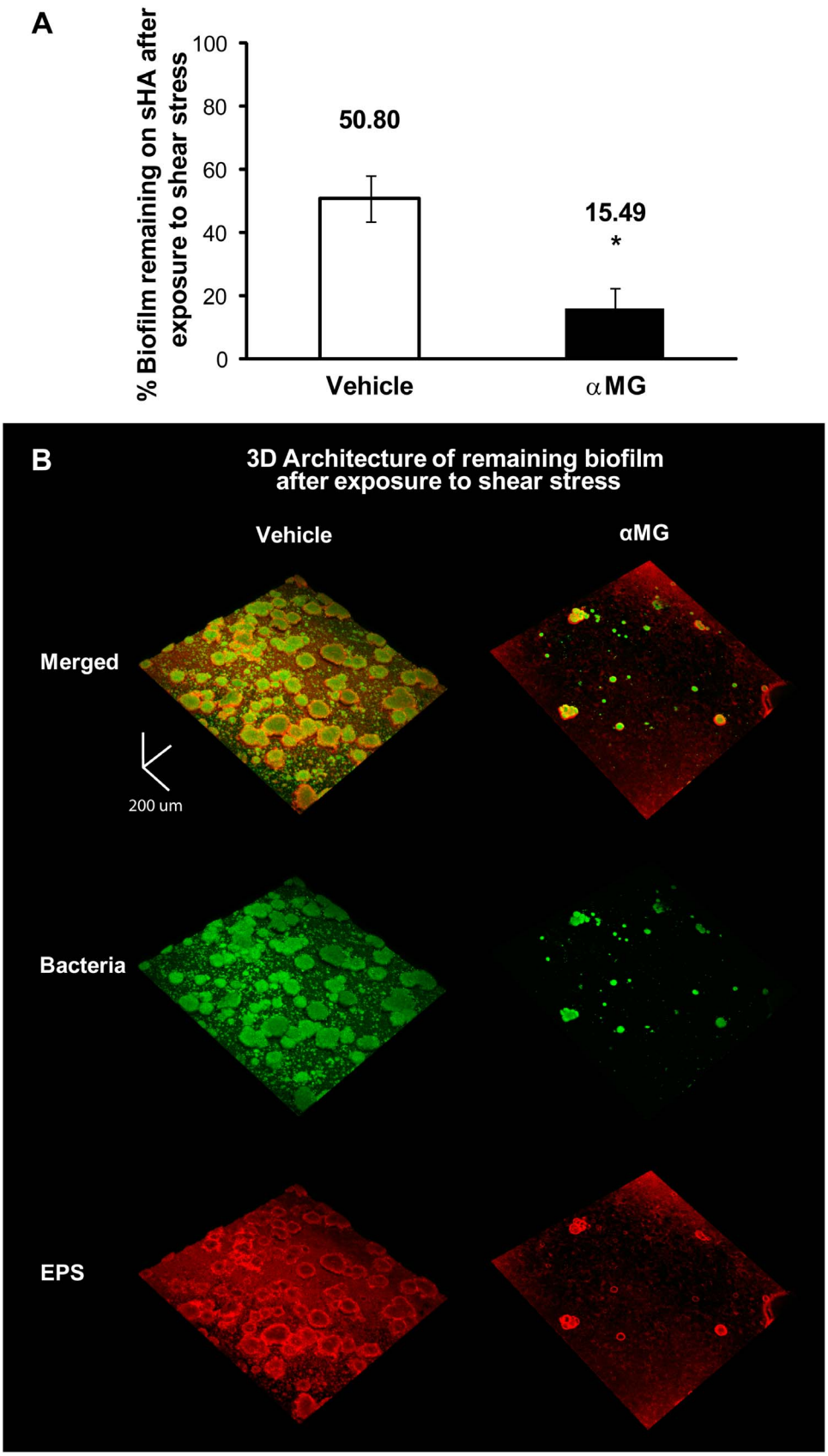

Figure 4. Biofilm mechanical stability following topical treatments. Panel A depicts the percentage of biomass of vehicle- or αMG-treated biofilms that remained on sHA after exposure to shear stress. The amount of biofilm dry-weight (biomass) before and after application of shear stress for each condition (vehicle- and αMG-treated) was determined, and the percentage of biofilm that remained on sHA disc surface was calculated. Data

are expressed as the mean ± one standard deviation. Values are significantly different from that for the vehicle control (n = 12; $P<0.05$, pair-wise comparison using Student's t test). Panel B shows representative 3D rendered images of treated-biofilms of *S. mutans* after shearing. The EPS channel is in red, and the bacterial cells are in green. Scale bars = 100 μm.
doi:10.1371/journal.pone.0111312.g004

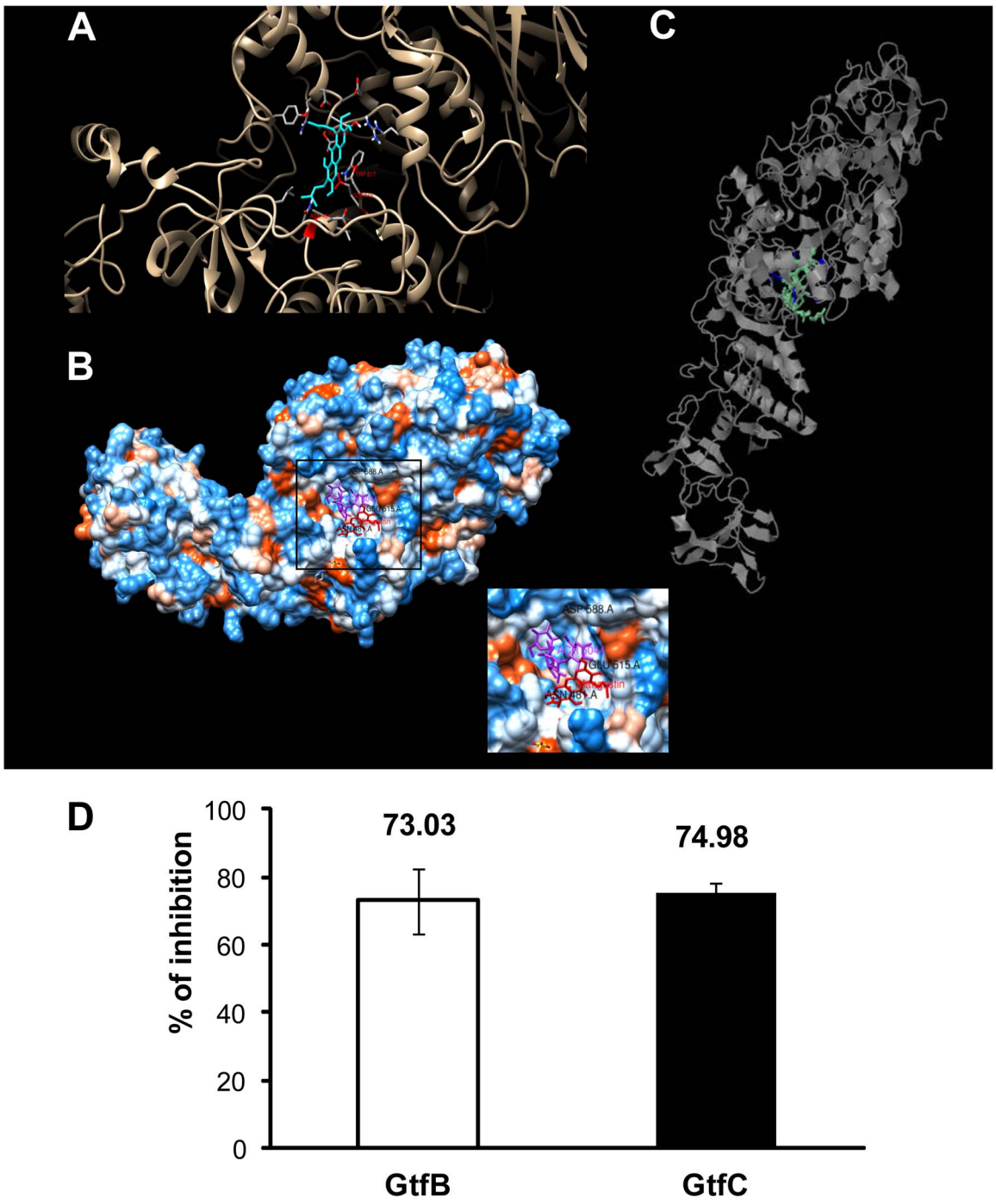

Figure 5. Snapshot of glucosyltransferase interaction with αMG compound and influence of 150 μM αMG on the activities of GtfB and GtfC. Panel A depicts the ribbon model of glucosyltransferase C (brown) docking α-mangostin (blue) using HEX-docking software Amino acids, such as Trp 517, Glu 515, Asp 588 and Asn 481 are interacting in the glucosyl binding site. Panel B depicts the surface model of glucosyltransferase C docking α-mangostin (red) and acarbose (purple) using HEX-docking software. Panel C depicts the glucosyltransferase B 3D ligand-binding site predicted model using Phyre Server. Panel D depicts Gtf activity of *S. mutans* cells when treated with αMG. The percentage of inhibition was calculated setting the vehicle control to 100% Gtf activity. Data are expressed as the mean ± one standard deviation. Values are significantly different from that for the vehicle control (n = 12; $P<0.05$, pair-wise comparison using Student's t test).
doi:10.1371/journal.pone.0111312.g005

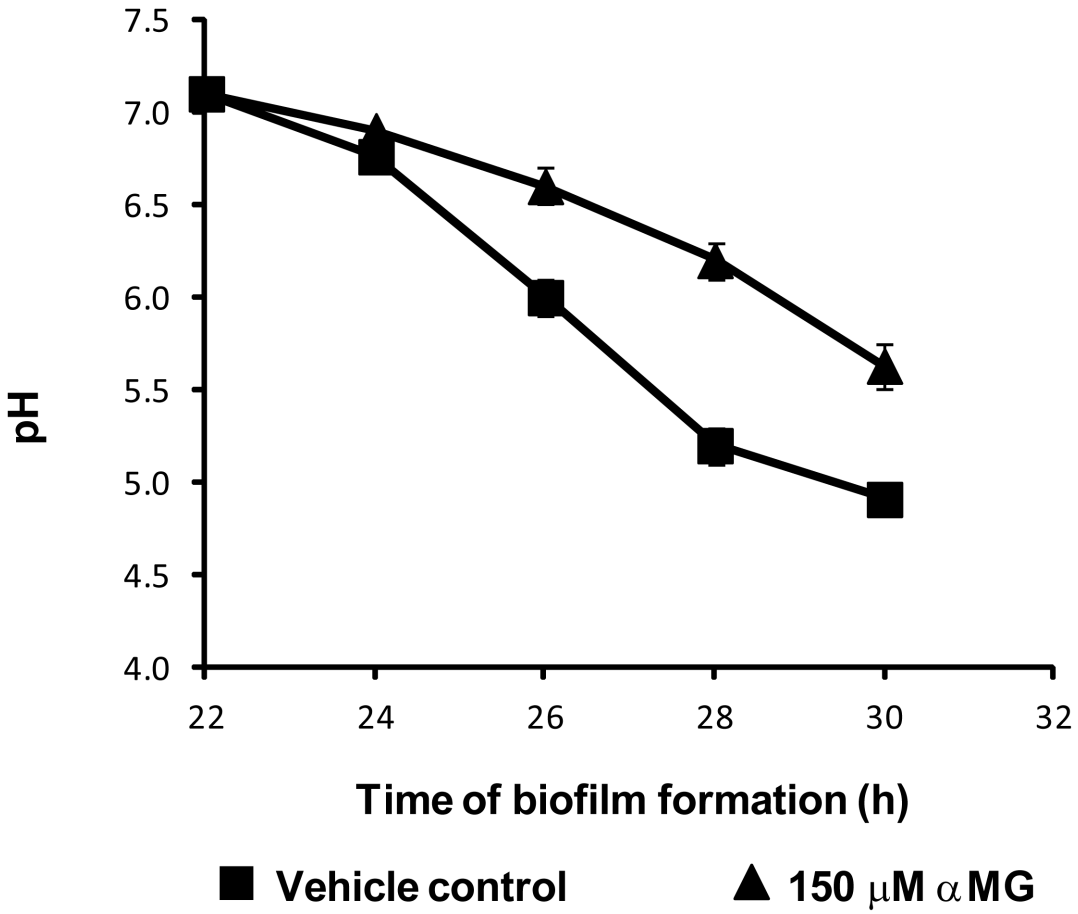

Figure 6. Effects of αMG on acid production by *S. mutans* UA159. Vehicle is represented by (■), while 150 μM αMG is represented by (▲). Data are expressed as the mean ± one standard deviation for experiments run in triplicates in at least three separate experiments.
doi:10.1371/journal.pone.0111312.g006

Statistical analyses

Data are presented as the mean ± one standard deviation (SD). Pair-wise comparisons were made between test and control using Student's t-test. Statistical analysis was performed using JMP (version 3.1; SAS Institute, Cary, NC). The level of significance was set at 5%.

Results and Discussion

αMG disrupts the accumulation and acidogenicity of *S. mutans* biofilms

In our experiment, *S. mutans* biofilms were initially treated with α-mangostin (αMG) at concentrations of 100, 150, and 200 μM (Table S1) based on bioactivity against planktonic *S. mutans* cells [27] and solubility in the vehicle system. We selected a concentration of 150 μM αMG, because it was as effective as 200 μM in reducing the overall biofilm development and acid production.

The data in Table 1 indicate that treatments with 150 μM αMG significantly reduced the accumulation of *S. mutans* biofilms on saliva-coated apatitic surfaces, which resulted in less biomass (dry-weight) and less total protein compared to the vehicle control ($P<0.05$). The viability of the biofilms was not significantly impacted by the treatments. Nevertheless, short-term topical applications (one-minute exposure, twice daily) significantly reduced the amount of polysaccharides in the biofilms (Table 1). The amount of insoluble exopolysaccharides (EPS) was drastically reduced, while the soluble EPS content was unaffected by αMG treatments. The data suggest that GtfB and GtfC, which are largely responsible for the synthesis of insoluble glucans in the biofilm matrix [8], could be targeted by αMG; while possibly having limited effects on the activity of GtfD (involved for soluble glucan synthesis). Interestingly, the amount of intracellular iodophilic polysaccharides (IPS), a glycogen-like storage polymer [46], was significantly disrupted by treatments with the agent.

Altogether, the biochemical changes inflicted by αMG may affect the matrix assembly and 3D biofilm architecture, which could disrupt the mechanical stability and adhesive strength of the treated biofilms.

αMG compromises the 3D architecture and mechanical stability of *S. mutans* biofilms

Confocal images revealed a marked impairment in the development of an insoluble EPS-matrix (in red), as well as the defective formation of bacterial clusters or microcolonies (in green) following αMG treatment, particularly at 44 h (Figure 3). The few microcolonies detected in the αMG-treated biofilms at 44 h visually appear to be larger than those treated with vehicle-control, suggesting that microcolony development was not completely inhibited. Nevertheless, the defective biofilm assembly resulted in an altered 3D architecture (at 68 h) characterized by sparsely distributed microcolonies (with many areas on the sHA surface

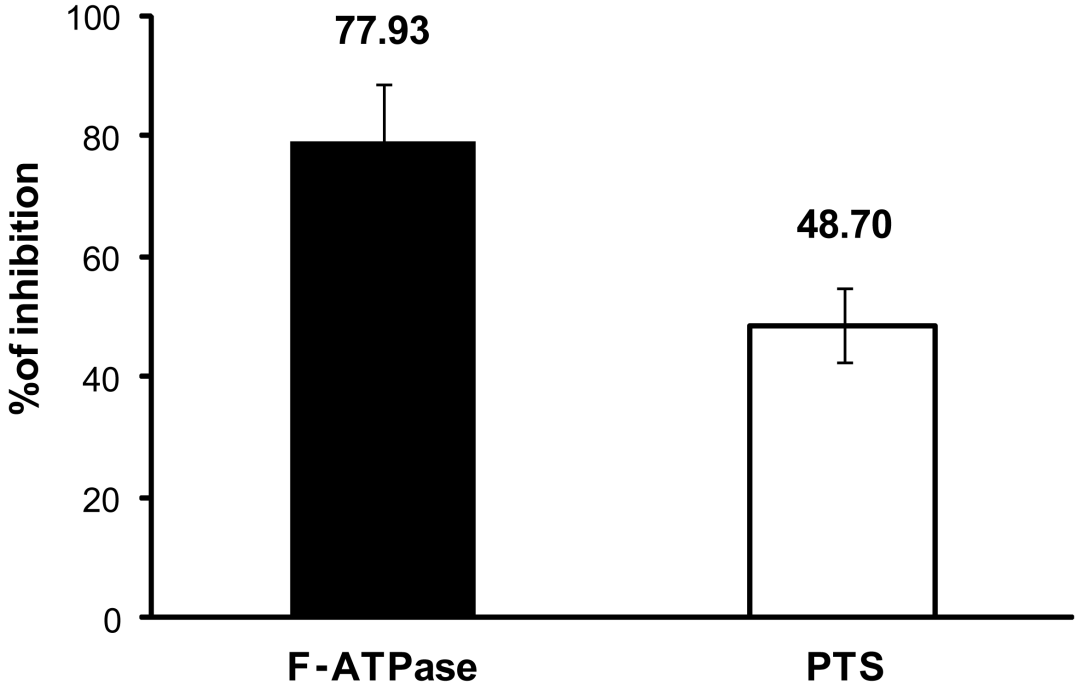

Figure 7. Effects of αMG on ATPase and PTS activities of *S. mutans* UA159. The percentage of inhibition was calculated setting the vehicle control to 100% enzymatic activity. Data are expressed as the mean ± one standard deviation. Values are significantly different from that for the vehicle control (n = 9; $P<0.05$, pair-wise comparison using Student's t test).
doi:10.1371/journal.pone.0111312.g007

that were devoid of such structures), as well as a less developed EPS matrix, compared to vehicle-treated biofilms. These findings agree well with our biochemical data showing a significant reduction in the insoluble EPS content.

These structural changes may affect the stability of the biofilms treated with αMG and facilitate mechanical clearance of biofilms. The mechanical stability of biofilms appears to be dependent on the exopolysaccharide content, as EPS binds the cells together while strengthening their cohesiveness [15,47–50]. Furthermore, glucans enhance *S. mutans* adhesive strength, while the development of multi-microcolony aggregates via EPS-cell adhesions provides structural integrity to *S. mutans* biofilms [16,18]. Thus, we hypothesized that the disruptive effects of αMG could facilitate biofilm removal and/or detachment. We investigated the impact of αMG on mechanical stability of *S. mutans* biofilms using a custom-built shear-inducing device (Figure S1).

The ability of treated-biofilms to withstand mechanical removal under shear stress was determined by measuring the amount of biofilm biomass (dry-weight) that remained on the sHA after shearing (Figure 4A). We observed that αMG-treated biofilms

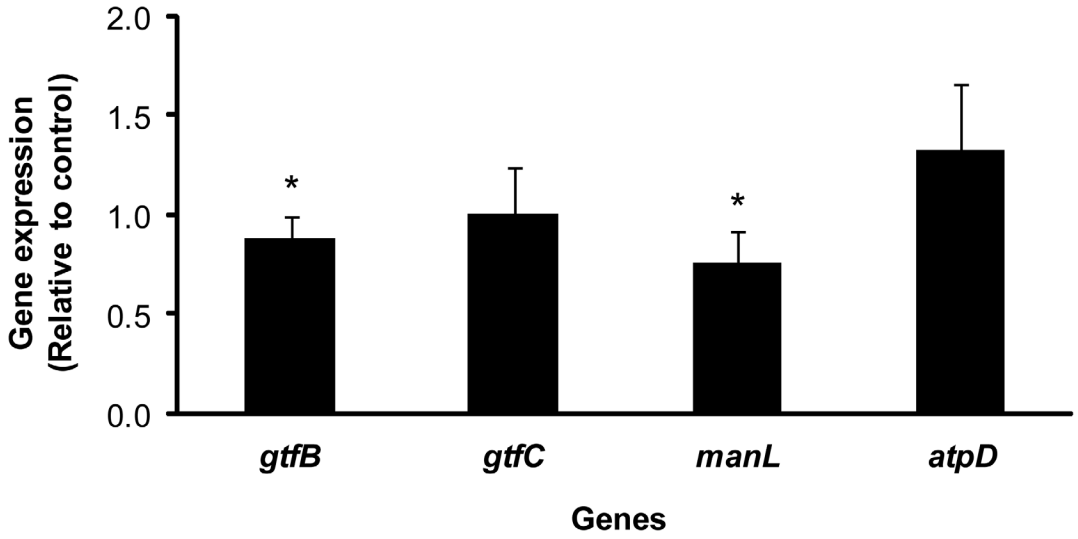

Figure 8. The expression of *S. mutans* genes *gtfB*, *gtfC*, *manL*, and *atpD* in biofilms. Fold changes ± one standard deviation. Values marked with asterisks are significantly different from that for the vehicle control (n = 8; $P<0.05$, pair-wise comparison using Student's t test).
doi:10.1371/journal.pone.0111312.g008

were more effectively removed from the sHA surface (84.51% removal) than those treated with vehicle-control (49.2%; $P<0.05$) when subjected to shear stress, indicating that the mechanical stability of the biofilms was compromised by αMG. Indeed, confocal images of αMG-treated biofilms show that most of the bacterial biomass and EPS was removed, while vehicle-treated biofilms show numerous EPS-enmeshed bacterial microcolonies still attached on the sHA surface (Figure 4B). Clearly, the data demonstrate that alterations in the EPS-matrix and microcolony assembly resulted in significantly less adherent biofilms, which facilitated their mechanical clearance from the sHA surface when exposed to shear force. By reducing the production of insoluble EPS, αMG treatments could affect optimal microcolony formation and surface anchoring as well as the cell-matrix cross-linking forces and the overall viscoelasticity, which have been shown to be critical for weakening the biofilm structure [18,49,51]. Further studies shall elucidate how αMG affects the adhesion forces and rheological properties of the biofilms locally.

αMG inhibits GtfB and GtfC activity

Previous studies have shown that extracellular glucans produced by GtfB and GtfC enzymes play vital, yet distinct roles in the formation of cariogenic biofilms and are essential in the pathogenesis of dental caries (as reviewed in Bowen and Koo [8]). The glucans synthesized by GtfC assemble the initial EPS layers on the sHA surface, which provide enhanced binding sites for *S. mutans* colonization and accumulation [52,53]. Conversely, the highly insoluble and structurally rigid glucans formed by GtfB embed the cells, contributing to the scaffolding of the 3D EPS-rich matrix [18]. The accumulation of Gtf-derived EPS and bacteria cells mediates the construction of EPS-enmeshed microcolonies that are firmly anchored to the apatitic surface [16–18,54]. Here, we examined whether αMG is capable of inhibiting the activity of purified GtfB and GtfC enzymes, which could explain the defective assembly and attachment of the treated biofilms observed in this study. Since there is no previous data on Gtf inhibition by αMG, we initially examined the likelihood of the agent to bind Gtfs using *in silico* docking studies.

Docking studies support the prediction of conformation and binding affinity for selected molecules against a given target protein [55]. Therefore, docking of αMG on Gtf was carried out to explore if/how this compound might interact with the enzymes. In our study, when the GtfC enzyme was docked with αMG, the energy value obtained by HEX software was −511.36 Kcal/mol, indicating a stable and strong binding between the two molecules [55]. The best docked structure, visualized by UCSF Chimera molecular modeling system version 1.8 (http://www.cgl.ucsf.edu/chimera/download.html), showed the interaction of four amino acids (Trp 517, Glu 515, Asp 588 and Asn 481) (Figure 5A and 5B). A previous report by Ito et al. [56] indicated that binding to Glu 515 compromised the acid/base catalyst function, while interaction with Trp 517 blocked the acceptor glycosyl moiety. These observations can explain the inhibitory properties shown by acarbose when bound to Gtf-SI [56]. As displayed in figure 5B, αMG and acarbose interact with Trp 517, which provides the main frame for the glycosyl acceptor binding site. Since the crystal structure of GtfB is not yet available, Phyre server [33] was used to predict ligand sites. The obtained results highlighted the presence of hydrophobic amino acids Leu 356, Gln 35, Ala 409, Lys 408, Asn 410; Asp 878, Ser 880; Ser 884, Leu 882, Tyr 936, Phe 881; Asn 1026 and some other amino acids with electrically charged amino acids like Asp 838I (Figure 5C).

All amino acids mentioned above are found in catalytic or the glucan binding regions of both GtfB and GtfC [57–60], suggesting that the function of these enzymes could be affected by αMG. Indeed, the enzymatic activity of purified GtfB and GtfC was impacted by αMG as shown in Figure 5D. The test agent was highly effective in reducing glucan synthesis by both enzymes, displaying more than 70% inhibition (vs. vehicle control) at 150 μM, which agrees well with the in silico analysis, as well as the biochemical (reduction of insoluble EPS content) and confocal imaging (defective assembly of EPS-matrix and impaired microcolony formation) data of the αMG-treated biofilms.

αMG affects acidogenicity of *S. mutans* biofilms, and disrupts F-ATPase and PTS activities

The biofilm EPS-matrix and microcolonies provide *S. mutans* with niches, where it survives and carries out glycolysis, even at low pH values, resulting in demineralization of the adjacent dental enamel [8,39]. In addition to the deleterious effects on biomass accumulation and structural organization, αMG also affected *S. mutans* biofilm acidogenicity following topical applications of the agent (Figure 6). αMG reduced both the acid production and the acid tolerance of *S. mutans* biofilm cells as indicated in the pH-drop profile (Figure 6). The test agent sensitized the biofilm cells to acidification to the point that the final pH value was significantly higher (~1 unit) than those treated with vehicle-control ($P<0.05$), suggesting that there may be disturbances in the activity of the proton-translocating membrane F-ATPase [27,39].

A previous study has shown that αMG was particularly effective in inhibiting the activity of $F(H^+)$-ATPase and PTS [27], which are critical for acid production and acid-tolerance and to ensure the optimum function of glycolysis by *S. mutans* within biofilms [61]. However, the assays were conducted with *S. mutans* grown in the planktonic phase. In this study, we examined the F-ATPase and PTS activity of biofilm cells following the treatment with αMG. The membrane-bound F-ATPase (H^+-translocating ATPase) is considered the primary determinant for acid tolerance [61]. During glycolysis, protons are pumped out of the cell by F-ATPase to help maintain ΔpH across the cell membrane, preventing acidification of the cytoplasm, which would typically inhibit intracellular enzymes [39]. Furthermore, under certain conditions, it also generates ATP for *S. mutans* growth and persistence [62]. The data in Figure 7 show that the F-ATPase activity was strongly inhibited by αMG with nearly 80% inhibition following topical treatments.

Conversely, sugar uptake by oral streptococci occurs primarily by means of the PTS system [63]. In this system, phosphoenol-pyruvate (PEP), provided by glycolysis, is cleaved by Enzyme I and the phosphate group is transferred to a general phosphocarrier protein, HPr, which in turn acts as a phosphate donor to membrane-bound Enzyme II [63]. Thus, the system catalyzes the transfer of phosphate to an incoming sugar and translocation of it across the cell membrane to yield a sugar phosphate in the cytoplasm, at which point sugar is metabolized via glycolytic pathways to produce organic acids. As shown in Figure 7, the PTS activity of biofilms treated with αMG was also significantly inhibited (~50% inhibition vs. vehicle-treated biofilms, $P<0.05$). Although the exact nature of αMG inhibition of the F-ATPase and PTS system found in this study remains to be determined using purified enzymes, our data suggest that αMG can affect *S. mutans* biofilms acidogenicity by disrupting the activity of these critical membrane-associated enzymes (albeit at concentrations of 3–5 times higher than those found against planktonic cells [27].

The inhibitory effects of αMG on F-ATPase and PTS could have additional impact on biofilm composition and virulence. Cytoplasmic acidification and reduction of sugar transport not only disrupts glycolytic acid production, but also the formation

and accumulation of intracellular iodophilic polysaccharides (IPS) [46], which could explain at least in part the marked reduction of IPS in the treated biofilms (Table 1). The role of IPS in *S. mutans* virulence and dental caries in general has been clearly documented [64–66]. IPS provides *S. mutans* with an endogenous source of carbohydrates that can be metabolized when exogenous fermentable substrates have been depleted within the oral cavity [67]. As a result, IPS can help to promote the formation of dental caries by prolonging the exposure of tooth surfaces to organic acids and a concomitant lower fasting pH in the matrix of the plaque [65]. Thus, the inhibition of IPS accumulation by αMG could also contribute with the overall disruptive effects of the agent on *S. mutans* biofilms acidogenicity.

αMG has limited effects on *gtfBC, atpD* and *manL* gene expression by *S. mutans* biofilms

Treatment of biofilms with α-mangostin could inhibit insoluble EPS synthesis and glycolytic pH drop in either of the following two ways: i) reducing enzymatic function and/or ii) affecting transcription of the genes encoding these enzymes to reduce the amount of enzyme produced. Therefore, we profiled the transcription of *gtfB, gtfC*, *atpD* (encoding F-ATPase), and *manL* (encoding a key component of the mannose PTS). The expression profiles of these genes are shown in Figure 8. Overall, RT-qPCR analysis showed only a slight repression of *gtfB* and *manL* after treatment with αMG ($P<0.05$), while no significant effects were observed on *gtfC* and *atpD* expression, suggesting that the reduction in EPS biomass in treated biofilms may be largely due to the impact on enzymatic function (Figure 5 and 7).

Upon biofilm establishment, the resident microorganisms, encased in an EPS-rich matrix, are difficult to remove or treat, while a highly acidogenic and aciduric biofilm environment is created [20]. In this paper, we reported that topical application of α-mangostin (αMG) can disrupt some of the major virulence properties of *S. mutans* within biofilms, impairing further biofilm accumulation and acidogenicity, while facilitating mechanical clearance. Although previous studies have shown the biological actions of αMG against planktonic cells of *S. mutans* and other organisms, this is the first study demonstrating the antibiofilm effects of this promising phytochemical agent. Analysis of our data shows that αMG could affect biofilm development by *S. mutans* through at least three distinctive and yet interconnected ways: 1) disruption of insoluble EPS-matrix assembly at least in part by inhibiting GtfB and GtfC enzymatic activities, 2) compromising the mechanical stability, which may be linked to defective EPS production and impaired microcolony formation (thereby facilitating biofilm detachment from sHA surface), and 3) reducing acidogenicity by affecting IPS accumulation and the activities of the F-ATPase and PTS system. The results from this study indicate that GtfB and GtfC, as well as the F-ATPase and PTS enzymatic systems, are therapeutic targets of αMG.

In conclusion, our study demonstrated that the phytochemical αMG may represent a potentially useful anti-virulence additive for the control and/or removal of cariogenic biofilms. Having shown here that αMG exhibits significant bioactivity against *S. mutans* biofilms, further understanding of the molecular mechanisms of action of this agent as well as its effects on mixed-species cariogenic biofilm models are certainly warranted. Furthermore, cytotoxicity studies revealed that αMG is non-toxic and is generally regarded as safe [68–70]. Clearly, the efficacy of our treatment needs to be evaluated *in vivo* using a rodent model of dental caries.

Supporting Information

Figure S1 Biofilm mechanical strength testing device. This supplementary material shows the design of the custom-built device to evaluate biofilm mechanical strength, and the principles of shear stress calculation.
(DOCX)

Table S1 Effects of α-mangostin on biofilm accumulation by *S. mutans* UA159.
(DOCX)

Acknowledgments

The authors are thankful to Marlise Klein and Stacy Gregoire for technical assistance during the gene expression and Gtfs assays.

Author Contributions

Conceived and designed the experiments: HK PTMN. Performed the experiments: PTMN GH MGB. Analyzed the data: PTMN GH MGB MF. Contributed to the writing of the manuscript: HK PTMN MF MGB.

References

1. Hall-Stoodley L, Stoodley P (2009) Evolving concepts in biofilm infections. Cell Microbiol 11: 1034–1043.
2. Dye BA, Tan S, Smith V, Lewis BG, Barker LK, et al. (2007) Trends in oral health status: United States, 1988–1994 and 1999–2004. Vital Health Stat 11: 1–92.
3. Marsh PD (2003) Are dental diseases examples of ecologicalcatastrophes? Microbiology 149: 279–294.
4. Flemmig TF, Beikler T (2011) Control of oral biofilms. Periodontol 2000 55(1): 9–15.
5. Jeon JG, Rosalen PL, Falsetta ML, Koo H (2011) Natural products in caries research: current (limited) knowledge, challenges and future perspective. Caries Res 45: 243–263.
6. Marsh PD (2013) Contemporary perspective on plaque control. Br Dent J 212(12): 601–606.
7. Paes Leme AF, Koo H, Bellato CM, Bedi G, Cury JA (2006) The role of sucrose in cariogenic dental biofilm formation-new insight. J Dent Res 85*:* 878–887.
8. Bowen WH, Koo H (2011) Biology of *Streptococcus mutans*-derived glucosyltransferases: role in extracellular matrix formation of cariogeneic biofilms. Caries Res 45: 69–86.
9. Nyvad B, Crielaard W, Mira A, Takahashi N, Beighton D (2013) Dental caries from a molecular microbiological perspective. Caries Res 47(2): 89–102.
10. Loesche WJ (1986) Role of *Streptococcus mutans* in human dental decay. Microbiol Rev 50: 353–380.
11. Quivey RG Jr, Kuhnert WL, Hahn K (2000) Adaptation of oral streptococci to low pH. Adv Microb Physiol 42: 239–74.
12. Burne RA, Marquis RE (2000) Alkali production by oral bacteria and protection against dental caries. FEMS Microbiol Lett 193(1): 1–6.
13. Smith EG, Spatafora GA (2012) Gene regulation in *S. mutans*: complex control in a complex environment. J Dent Res 91(2): 133–141.
14. Lemos JA, Quivey RG Jr, Koo H, Abranches J (2013) *Streptococcus mutans*: a new Gram-positive paradigm? Microbiology 159(Pt 3): 436–445.
15. Vinogradov AM, Winston M, Rupp CJ, Stoodley P (2004) Rheology of biofilms formed from the dental plaque pathogen *Streptococcus mutans*. Biofilms 1: 49–56.
16. Cross SE, Kreth J, Zhu L, Sullivan R, Shi W, et al. (2007) Nanomechanical properties of glucans and associated cell-surface adhesion of *Streptococcus mutans* probed by atomic force microscopy under in situ conditions. Microbiology 153: 3124–3132.
17. Kreth J, Zhu L, Merritt J, Shi W, Qi F (2008) Role of sucrose in the fitness of *Streptococcus mutans*. Oral Microbiol Immunol 23(Pt 12): 213–219.
18. Xiao J, Klein MI, Falsetta ML, Lu B, Delahunty CM, et al. (2012) The exopolysaccharide matrix modulates the interaction between 3D architecture and virulence of a mixed-species oral biofilm. PLoS Pathog 8: e1002623.
19. Hope CK, Wilson M (2004) Analysis of the effects of chlorhexidine on oral biofilm vitality and structure based on viability profiling and an indicator of membrane integrity. Antimicrob Agents Chemother 48: 1461–1468.
20. Koo H, Falsetta ML, Klein MI (2013) The exopolysaccharide matrix: a virulence determinant of cariogenic biofilm. J Dent Res 92(12): 1065–73.
21. Vroom JM, De Grauw KJ, Gerritsen HC, Bradshaw DJ, Marsh PD, et al. (1999) Depth penetration and detection of pH gradients in biofilms by two-photon excitation microscopy. Appl Environ Microbiol 65: 3502–3511.

22. Guo L, Hu W, He X, Lux R, McLean J, et al. (2013) Investigating acid production by *Streptococcus mutans* with a surface-displayed pH sensitive green fluorescent protein. PLoS One 8: e57182.
23. Li Y, Burne RA (2001) Regulation of the *gtfBC* and *ftf* genes of *Streptococcusmutans* in biofilms in response to pH and carbohydrate. Microbiology 147(Pt 10): 2841–2848.
24. Ee GC, Daud S, Taufiq-Yap YH, Ismail NH, Rahmani M (2006) Xanthones from *Garcinia mangostana* (Guttiferae). Nat Prod Res 20: 1067–1073.
25. Ee GC, Daud S, Izzaddin SA, Rahmani M (2008) *Garcinia mangostana*: a source of potential anti-cancer lead compounds against CEM-SS cell line. J Asian Nat Prod Res 10: 475–479.
26. Jung HA, Su BN, Keller WJ, Mehta RG, Kinghorn AD (2006) Antioxidant xanthones from the pericarp of *Garcinia mangostana* (Mangosteen). J Agric Food Chem 54: 2077–2082.
27. Nguyen PTM, Marquis RE (2011) Antimicrobial actions of alpha-mangostin against oral Streptococci. Can J Microbiol 57: 217–25.
28. Koo H, Hayacibara MF, Schobel BD, Cury JA, Rosalen PL, et al. (2003) Inhibition of *Streptococcus mutans* biofilm accumulation and polysaccharide production by apigenin and tt-farnesol. J Antimicrob Chemother 52: 782–789.
29. Koo H, Schobel B, Scott-Anne K, Watson G, Bowen WH, et al. (2005) Apigenin and tt-farnesol with fluoride effects on *Streptococcus mutans* biofilms and dental caries. J Dent Res 84(11): 1016–20.
30. Koo H, Nino de Guzman P, Schobel BD, Vacca Smith AV, Bowen WH (2006) Influence of cranberry juice on glucan-mediated processes involved in *Streptococcus mutans* biofilm development. Caries Res 40(1): 20–7.
31. Heydorn A, Nielsen AT, Hentzer M, Sternberg C, Givskov M, et al. (2000) Quantification of biofilm structures by the novel computer program COMSTAT. Microbiology 146: 2395–2407.
32. Koo H, Xiao J, Klein MI, Jeon JG (2010) Exopolysaccharides produced by *Streptococcus mutans* glucosyltransferases modulate the establishment of microcolonies within multispecies biofilms. J Bacteriol 192: 3024–3032.
33. Kelley LA, Sternberg MJ (2009) Protein structure prediction on the Web: a case study using the Phyre server. Nat Protoc 4: 363–371.
34. Koo H, Vacca Smith AM, Bowen WH, Rosalen PL, Cury JA, et al. (2000) Effects of Apis mellifera propolis on the activities of streptococcal glucosyltransferases in solution and adsorbed ontosaliva-coated hydroxyapatite. Caries Res 34(5): 418–426.
35. Venkatraman V, Ritchie DW (2012) Flexible protein docking refinement using pose-dependent normal mode analysis. Proteins 80(9): 2262–74.
36. Ritchie DW, Kemp GJ (2000) Protein docking using spherical polar fourier correlations. Proteins 39: 178–94.
37. Ritchie DW, Venkatraman V (2010) Ultra-fast FFT protein docking on graphics processors. Bioinformatics 26: 2398–405.
38. Macindoe G, Mavridis L, Venkatraman V, Devignes MD, Ritchie DW (2010) HexServer: an FFT-based protein docking server powered by graphics processors. Nucleic Acids Res. 38(Web Server issue): W445–9.
39. Belli WA, Marquis RE (1991) Adaptation of *Streptococcus mutans* and *Enterococcus hirae* to acid stress in continuous culture. Appl Environ Microbiol 57: 1134–1138.
40. Phan TN, Buckner T, Sheng J, Baldeck JD, Marquis RE (2004) Physiologic actions of zinc related to inhibition of acid and alkali production by oral streptococci in suspensions and biofilms. Oral Microbiol Immunol 19(1): 31–8.
41. Cury JA, Koo H (2007) Extraction and purification of total RNA from *Streptococcus mutans* biofilms. Anal Biochem 365: 208–14.
42. Yin JL, Shackel NA, Zekry A, McGuinness PH, Richards C, et al. (2001) Real-time reverse transcriptase-polymerase chain reaction (RT-PCR) for measurement of cytokine and growth factor mRNA expression with fluorogenic probes or SYBR green. Immunol Cell Biol 79: 213–222.
43. Klein MI, DeBaz L, Agidi S, Lee H, Xie G, et al. (2010) Dynamics of *Streptococcus mutans* transcriptome in response to starch and sucrose during biofilm development. PLoS One 5: e13478.
44. Bustin SA, Benes V, Garson JA, Hellemans J, Huggett J, et al. (2009) The MIQE guidelines: minimum information for publication of quantitative real-time PCR experiments. Clin Chem 55: 611–622.
45. Falsetta ML, Klein MI, Lemos JA, Silva BB, Agidi S, et al. (2012) Novel antibiofilm chemotherapy targets exopolysaccharide synthesis and stress tolerance in *Streptococcus mutans* to modulate virulence expression in vivo. Antimicrob Agents Chemother 56: 6201–6211.
46. Hamilton IR (1990) Biochemical effects of fluoride on oral bacteria. J Dent Res 69 (spec issue): 660–667.
47. Körstgens V, Flemming HC, Wingender J, Borchard W (2001) Uniaxial compression measurement device for investigation of the mechanical stability of biofilms. J Microbiol Methods. 46(1): 9–17.
48. Cense AW, Peeters EA, Gottenbos B, Baaijens FP, Nuijs AM, et al. (2006) Mechanical properties and failure of *Streptococcus mutans* biofilms, studied using a microindentation device. J Microbiol Methods 67(3): 463–472.
49. Jones WL, Sutton MP, Mckittrick L, Stewart PS (2011) Chemical and antimicrobial treatments change the viscoelastic properties of bacterial biofilms Biofouling 27: 207–15.
50. Waters MS, Kundu S, Lin NJ, Lin-Gibson S (2014) Microstructure and mechanical properties of in situ *Streptococcus mutans* biofilms. ACS Appl Mater Interfaces 6(1): 327.
51. Simoes M, Pereira MO, Vieira MJ (2004) Effect of cationic surfactants on biofilm removal and mechanical stability. International Conference on Biofilm 2014: Structure and activity of biofilm Las Vegas, NV, USA. 171–175.
52. Schilling KM, Bowen WH (1992) Glucans synthesized in situin experimental salivary pellicle function as specific binding sites for *Streptococcus mutans*. Infect Immun 60: 284–295.
53. Venkitaraman AR, Vacca-Smith AM, Kopec LK, Bowen WH (1995) Characterization of glucosyltransferaseB, GtfC, and GtfD in solution and on the surface of hydroxyapatite. J Dent Res 74(10): 1695–1670.
54. Xiao J, Koo H (2010) Structural organization and dynamics of exopolysaccharide matrix and microcolonies formation by *Streptococcus mutans* in biofilms. J Appl Microbiol 108: 2103–2113.
55. Gundampati RK, Sahu S, Sonkar KS, Debnath M, Srivastava AK, et al. (2013) Modeling and molecular docking studies on RNase *Aspergillus niger* and *Leishmania donovani* actin: antileishmanial activity. Am J Biochem Biotechnol 9(3): 318–328.
56. Ito K, Ito S, Shimamura T, Weyand S, Kawarasaki Y, et al. (2011) Crystal structure of glucansucrase from the dental caries pathogen *Streptococcus mutans*. J Mol Biol 408(2): 177–186.
57. Monera D, Sereda TJ, Zhou NE, Kay CM, Hodges RS (1995) Relationship of side chain hydrophobicity and alpha-helical propensity on the stability of the single-stranded amphipathic alpha-helix. J Pept Sci 1: 319–329.
58. Monchois V, Willemot RM, Monsan P (1999) Glucansucrases: mechanism of action and structure-function relationships. FEMS Microbiol Rev 23: 131–151.
59. Colby SM, Russell RRB (1997) Sugar metabolism by mutans streptococci. Soc Appl Bacteriol Symp 26: 80S–88S.
60. Mooser G, Hefta SA, Paxton RJ, Shively JE, Lee TD (1991) Isolation and sequence of an active-site peptide containing a catalytic aspartic acid from two *Streptococcus sobrinus* alpha-glucosyltransferases. J Biol Chem 266: 8916–22.
61. Marquis RE, Clock SA, Mota-Meira M (2003) Fluoride and organic weak acids as modulators of microbial physiology. FEMS Microbiol Rev 26: 493–510.
62. Lemos JA, Abranches J, Burne RA (2005) Responses of cariogenic streptococci to environmental stresses. Curr Issues Mol Biol 7: 95–10.
63. Burne RA, Ahn SJ, Wen ZT, Zeng L, Lemos JA, et al. (2009) Opportunities for disrupting cariogenic biofilms. Adv Dent Res 21(1): 17–20.
64. Loesche WJ, Henry CA (1967) Intracellular microbial polysaccharide production and dental caries in a Guatemalan Indian village. Archs Oral Biol 12: 189–194.
65. Tanzer JM, Freedman ML, Woodiel FN, Eifert RL, Rinehimer LA (1976) Association of Streptococcus mutans virulence with synthesis of intracellular polysaccharide. In: Proceedings in microbiology. Aspects of dental caries. Stiles HM, Loesche WJ, O'Brien TL, editors. Special supplement to Microbiology Abstracts, vol. 3. Information Retrieval, Inc. London, 596–616.
66. Spatafora G, Rohrer K, Barnard D, Michalek SA (1995) *Streptococcus mutans* mutant that synthesizes elevated levels of intracellular polysaccharide is hypercariogenic in vivo. Infect Immun 63(7): 2556–263.
67. Hamilton IR (1976) Intracellular polysaccharide synthesis by cariogenic microorganisms. In: Proceedings in microbiology. Aspects of dental caries. Stiles HM, Loesche WJ, O'Brien TL, editors. Special supplement to Microbiology Abstracts. Vol. 3. London: Information Retrieval, Inc., 683–701.
68. Kaomongkolgit R, Jamdee K, Chaisomboon N (2009) Antifungal activity of α-mangostin against *Candida albicans*. J Oral Sci 51(3): 401–406.
69. Obolskiy D, Pischel I, Siriwatanametanon N, Heinrich M (2009) *Garcinia mangostana* L.: a phytochemical and pharmacological review. Phytother Res 23(8): 1047–1065.
70. Kosem N, Ichikawa K, Utsumi H, Moongkarndi P (2013) In vivo toxicity and antitumor activity of mangosteen extract. J Nat Med 67(2): 255–263.